

Enhanced thermoelectric cooling at cold junction interfaces

U. Ghoshal,^{a)} S. Ghoshal, C. McDowell, and L. Shi
 IBM Research, Austin Research Laboratory, Austin, Texas 78758

S. Cordes and M. Farinelli
 IBM Research, T.J. Watson Research Center, Yorktown Heights, New York 10598

(Received 21 January 2002; accepted for publication 25 February 2002)

We describe a thermoelectric device structure that confines the thermal gradients and electric fields at the boundaries of the cold end, and exploits the reduction of thermal conductivity at the interfaces and the poor electron-phonon coupling at the junctions. The measured temperature–current and voltage–current characteristics of a prototype cold point-contact thermoelectric cooler based on a *p*-type $\text{Bi}_{0.5}\text{Sb}_{1.5}\text{Te}_3$ and *n*-type $\text{Bi}_2\text{Te}_{2.9}\text{Se}_{0.1}$ material system indicate an enhanced thermoelectric figure-of-merit ZT in the range of 1.4–1.7 at room temperature. © 2002 American Institute of Physics. [DOI: 10.1063/1.1473233]

Solid-state thermoelectric coolers can revolutionize thermal management of electronics and optoelectronic systems, and small-scale refrigeration if the coolers could attain thermodynamic efficiency greater than 30% of the ideal Carnot cycle. The maximum temperature differential and the efficiency of thermoelectric coolers¹ are known to depend on material properties through the thermoelectric figure-of-merit $ZT = S^2\sigma T/\lambda$. Z has units of inverse temperature, and depends on the Seebeck coefficient S , the electrical conductivity σ , the thermal conductivity λ , and the temperature T . The efficiency requirements imply the figure-of-merit needs to be increased from $ZT \sim 1$ typical of bismuth chalcogenides to $ZT > 3$. A variety of promising approaches such as transport and confinement in nanowires and quantum dots, reduction of thermal conductivity in the direction perpendicular to superlattice planes, and optimization of ternary or quaternary chalcogenides and skutteridites have been investigated recently.^{2,3} We have been investigating the scaling properties of thin-film thermoelectric coolers, and the properties of structured point contacts at the cold end.⁴ This letter illustrates an example of the latter approach for increasing the thermoelectric figure-of-merit.

In order to confine the thermoelectric problem at the surfaces, we structured the cold end as an array of metallic point contacts that are sandwiched between *n*-type and *p*-type thermoelectric elements [Fig. 1(a)]. The electric field and temperature gradients are localized within distances of the order of the individual tip radius r_0 if the interface and spreading electrical and thermal resistances are much larger than the bulk (body) resistance of the thermoelements. It can be shown that a conservative criterion is $p > \sqrt{2\pi r_0 t}$, p being the distance between the points and t being the thickness of the thermoelements. The field localization to spatial scales of the order of the tip radius can eliminate the requirement of thick substrates and lower the manufacturing cost of a thin-film process.

The microscopic structure of the point contacts varies between the two extreme scenarios depicted in Fig. 1(b). In

one extreme, the contact is primarily by electronic tunneling through a gap wherein the phonon coupling via near-field coupling is negligible. The electrons injected into the thermoelements are not in thermal equilibrium with the phonon system for a finite distance Λ from the surface. The coupled equations for heat transfer for the electron-phonon system near the surface of the thermoelements are

$$P(T_e - T_p) - \nabla(\lambda_e \nabla T_e) - \frac{|J|^2}{\sigma} = 0,$$

$$P(T_p - T_e) - \nabla(\lambda_{sp} \nabla T_p) = 0, \quad (1)$$

where the parameter P represents the intensity of the electron-phonon interaction,^{5,6} J is the local current density, T_e and T_p denote the electron temperature and phonon temperature, respectively, σ is the electrical conductivity, λ_e is the electronic thermal conductivity, and λ_{sp} is the surface lattice thermal conductivity. We have solved the radially symmetric coupled Eqs. (1) subject to zero phonon-based heat conduction $\lambda_{sp} dT_p/dr = 0$ and $T_e = T_s$ at the surface, and the constraint $T_e(r), T_p(r) \rightarrow T_h$ at large distances from the point contact. The solution indicates that the characteristic thermalization length Λ can be expressed as Λ

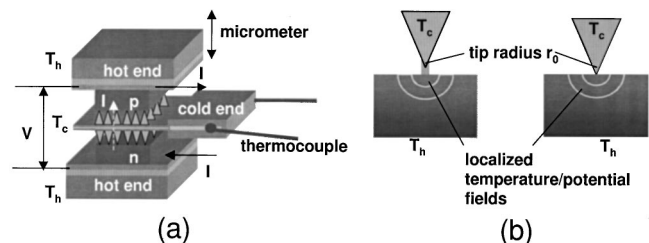


FIG. 1. (a) The physical structure of a cold point contact thermoelectric cooler investigated in the experiments. A thermocouple is attached to the cold end for direct measurement of temperature differential ΔT based on the thermocouple voltage. The voltage–current characteristics are measured using four leads, two for supplying the current I through the cooler and two for the device voltage V . (b) Schematic illustration of two limiting cases for operation of a cold point contact with tip radius r_0 : first, the electronic tunneling regime with negligible phonon conduction, and second, the case where tip is in physical contact with the surface and there is a finite phonon conduction.

^{a)}Author to whom correspondence should be addressed; electronic mail: ghoshal@us.ibm.com

$=\sqrt{\lambda_e\lambda_{sp}/[(\lambda_e+\lambda_{sp})P]}$ and the nonequilibrium effects result in a reduced thermal conductivity λ at the point contact

$$\lambda = \frac{\lambda_e(1+r_0/\Lambda)(1+\lambda_e/\lambda_{sp})}{1+(\lambda_e/\lambda_{sp})(1+r_0/\Lambda)}. \quad (2)$$

As $r_0/\Lambda \rightarrow \infty$, $\lambda \rightarrow \lambda_{sp} + \lambda_e$ and as $r_0/\Lambda \rightarrow 0$, $\lambda \rightarrow \lambda_e$. The characteristic thermalization length Λ is about 300 nm^5 for our material system. The equations indicate that sharp cold point contacts in the tunneling mode operate in the phonon-glass-electron-crystal limit: $ZT \rightarrow S^2\sigma T/\lambda_e = S^2/L_0$, where L_0 is the Lorenz number for the thermoelectric materials under consideration ($\sqrt{L_0} \sim 125 \mu\text{V/K}$ for $\text{Bi}_{0.5}\text{Sb}_{1.5}\text{Te}_3$). In the other extreme, the metal tip compresses the surface of the thermoelement and the transport is dependent on both electronic tunneling and phonon conduction. The finite heat conduction by phonons at the tip results in lowering of the phonon temperature at the surface, and $\lambda \approx \lambda_{sp} + \lambda_e$. Note that the surface lattice thermal conductivity λ_{sp} is lower than the bulk thermal conductivity due to Kapitza boundary effects and less understood pressure/stress effects that affect phonon scattering at point contacts. Pressure effects could also increase the local Seebeck coefficients in p -type $\text{Bi}_{0.5}\text{Sb}_{1.5}\text{Te}_3$.⁷ The metal point contacts utilized in these experiments had $r_0 = 0.6 \mu\text{m}$. Assuming $\lambda_e = \sigma L_0 T_a = 0.47 \text{ W/mK}$, $\lambda_{sp} = 1.2 \text{ W/mK}$, and $\Lambda = 300 \text{ nm}$ (or equivalently, $\lambda_e/\lambda_{sp} \sim 0.4$, $r_0/\Lambda \sim 2$) the thermal conductivity λ at the point contact would decrease from $1.4 \lambda_{sp}$ to $0.76 \lambda_{sp}$ in the tunneling scenario of Fig. 1(b). However, the nonplanarity of the thermoelectric surfaces and the variations in the heights of the point contacts result in a substantial number of points physically contacting the surface as in the second scenario of Fig. 1(b).

The p -type substrates used in the experiments were cleaved from a polycrystalline $\text{Bi}_{0.5}\text{Sb}_{1.5}\text{Te}_3$ alloy sample while the surface of the n -type $\text{Bi}_2\text{Te}_{2.9}\text{Se}_{0.1}$ substrates were mechanically polished. The Seebeck coefficients S_0 and the electrical conductivity σ of the thermoelements were nominally $210 \mu\text{V/K}$ and $0.1 \text{ S}/\mu\text{m}$, respectively, and the nominal thicknesses t were $100 \mu\text{m}$. Before assembly of the cooler, the surfaces were cleaned by a solution of hydrochloric acid and nitric acid ($\text{HCl}:\text{HNO}_3:\text{H}_2\text{O}::1:1:2$ by volume), and rinsed with de-ionized water. The hot ends of the thermoelements were soldered to Ni-coated copper strips by Ostalloy (50% Bi, 26.7% Pb, 13.3% Sn, 10% Cd) that melted at 343 K. The process flow utilized for the fabrication of the metal cold points is outlined in Fig. 2(a). A Si mold for the metal cold points is first fabricated by patterning oxidized Si wafer, wet etching in alcohol-rich phase of a isopropyl alcohol/KOH bath to create Si pits, and then removing the oxide layers by etching in buffered HF solution. A 100 nm Cu seed layer is sputtered onto the pits without any intermediate adhesion layer. Next, a 25 μm layer of Cu, a 5 μm layer of Ni, and a 5 μm layer of Au are electroplated on the seed layer. The metal Cu/Ni/Au layers are peeled out from the Si mold by ultrasound wave agitation in alcohol. The metal cold point foils were then diced and folded around the junction of a thermocouple⁸ with a wire diameter of 50 μm to form the cold end. The cold points were then sandwiched between the thermoelements using micropositioners. Figure 2(b) illustrates a scanning electron microscopy micrograph of a cold

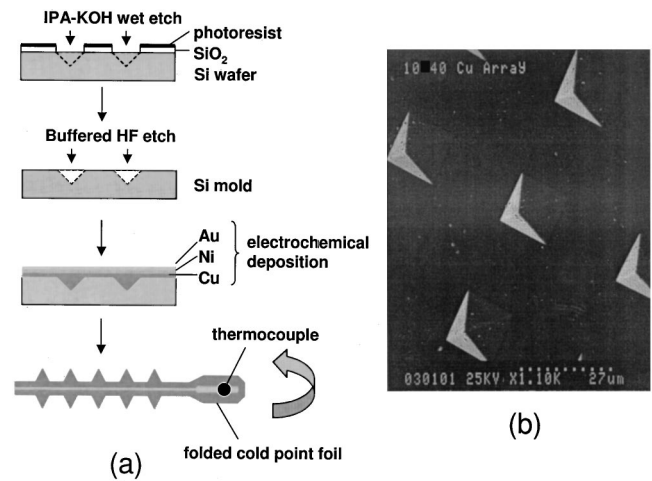


FIG. 2. (a) The process flow for the fabrication of the metal cold point structure investigated in the experiments. (b) Scanning electron microscope micrograph of a cold point array with a pitch of $40 \mu\text{m}$, tip radius of $0.5 \mu\text{m}$, and a square base of $10 \times 10 \mu\text{m}^2$.

point array with a pitch of $40 \mu\text{m}$. The individual pyramidal structures had a tip radius of $0.5 \mu\text{m}$ with a square base of $10 \times 10 \mu\text{m}^2$.

We measured the performance of $p+n$ coolers [Fig. 1(a)] in a vacuum ($\sim 3 \text{ mTorr}$) bell jar housing a two-axis micrometer. The use of vacuum is not fundamental to the operation of the cold point coolers, but it was necessary to avoid thermal shorting due to air conduction for the array point density explored in this set of experiments. The heat load at the cold end consisted of conduction loss due to the two leads of the thermocouple and radiation loss due to a thermocouple leads and a peripheral overhang. Figure 3 shows typical maximum temperature differential-current and four-point voltage-current data for an 80×80 array of cold points at a pitch of $20 \mu\text{m}$ with tip radius of $0.6 \mu\text{m}$. With the hot end constrained at ambient temperature $T_a = 296.5 \text{ K}$, the heat balance at the cold end for a temperature differential ΔT is achieved when $S(T_a - \Delta T)I - \frac{1}{2}I^2R - K\Delta T = 0$, where $S = S_p + |S_n|$, $R = R_n + R_p$, and $K = K_n$

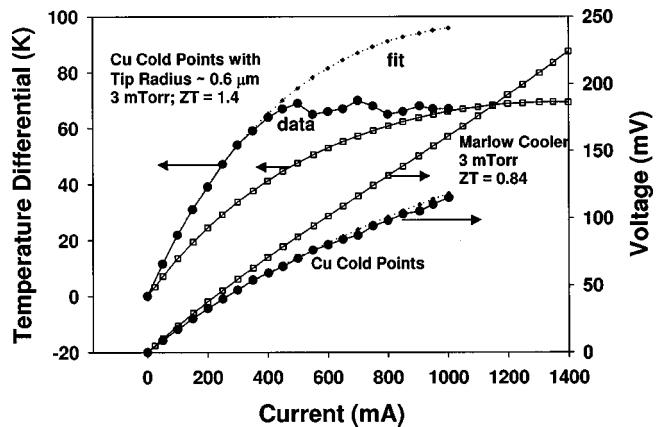


FIG. 3. The temperature differential ΔT and the device voltage V plotted as a function of the device current I . The measurements were performed in vacuum to avoid the thermal conduction by air and condensation effects. The solid lines correspond to the measured data while the dotted lines represent the best fit to Eq. (3). The 80×80 array of cold points had a pitch of $20 \mu\text{m}$ and tip radius of $0.6 \mu\text{m}$. The performance of a two-element $n+p$ conventional thermoelectric cooler fabricated by Marlow Industries, Inc. is shown for reference.

$+K_p+K_{\text{load}}$ are the sum of the Seebeck coefficients, electrical resistances, and thermal conductances of the n -type and p -type thermoelements, respectively. The maximum temperature differential and the voltage across the thermoelement are

$$\Delta T = \frac{ST_a I - \frac{1}{2} I^2 R}{K + SI}, \quad (3)$$

$$V = IR + S\Delta T.$$

A nonlinear curve fit to the $\Delta T-I$ and $V-I$ data using the Eqs. (3) results in the following parameters: $S=440 \mu\text{V/K}$, $R=76 \text{ m}\Omega$, and $K=0.54 \text{ mW/K}$ or $ZT_a=S^2 T_a/(KR)=1.4$. The fit has less than 0.1% error for $\Delta T < 60 \text{ K}$. The extracted value of the Seebeck coefficient $S \approx 2S_0$. At low current density and smaller temperature differentials, the coolers operate at thermodynamic efficiency of 17%–21%—significantly better than conventional ones. We do not yet fully understand the factors that limit the temperature differential in the cold point coolers to 70–75 K at high currents. Figure 3 also compares the performance of the cold point coolers to a two element $n+p$ thermoelectric cooler fabricated by Marlow Industries, Inc. and tested in the same setup under similar conditions. The length of the Marlow thermoelements was 1.52 mm and the cross section area was $0.63 \times 0.63 \text{ mm}^2$.

The thermal parasitics due to radiation losses need to be accounted to estimate the intrinsic ZT . The major contributors to radiation loss were the 2 cm long $50 \mu\text{m}$ diameter wires of the thermocouple, and the 8.88 mm^2 overhang that held the thermocouple at the cold end. We estimate the parasitic radiation conductance by the relation $K_r=4\sigma_B A_r T_a^3$ where σ_B is the Stefan–Boltzmann constant and A_r is the net surface area. $K_r=92.8 \mu\text{W/K}$ for the device geometry tested. Hence, we estimate the intrinsic $Z_i T_a=S^2 T_a/[(K-K_r)R]=1.69$. This value of the intrinsic $Z_i T_a$ was supported by another independent experiment that exploited the fact that thermal conduction by air suppresses the cooling effects in arrays with low density of cold points. The differential electrical resistance for small currents is given by

$$\left. \frac{\partial V}{\partial I} \right|_{I \rightarrow 0} = R + S \left. \frac{\partial \Delta T}{\partial I} \right|_{I \rightarrow 0} = R + \frac{S^2 T_a}{K}. \quad (4)$$

For a sparse array in which thermal conduction by air is the dominant contributor to K , the differential resistance for small currents is simply the ohmic resistance R . Hence, in such cases

$$Z_i T_a = \frac{\partial V / \partial I|_{\text{vacuum}} - \partial V / \partial I|_{\text{air}}}{\partial V / \partial I|_{\text{air}}}. \quad (5)$$

Figure 4 shows the differential resistance at low currents and the $Z_i T_a$ extracted from a $p+n$ cooler with a 40×40 array of cold points at a pitch of $40 \mu\text{m}$ subjected to pressure cycles

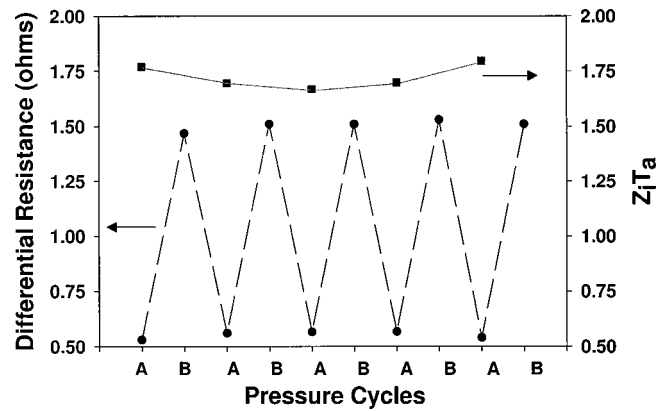


FIG. 4. Direct determination of intrinsic $Z_i T_a$ by measuring the differential resistance at small currents of a structure incorporating a 40×40 array of cold points at a pitch of $40 \mu\text{m}$. The measurement corresponding to ambient atmospheric pressure is denoted by A and that in vacuum ($< 3 \text{ mTorr}$) is denoted by B.

between ambient atmospheric pressure and vacuum, with an optimized adjustment of the micrometer. The cold end structure did not include the thermocouple or the overhang, and minimized the radiation parasitics. $Z_i T_a \sim 1.7$ measured by this method agrees well with the estimates derived earlier. The effective pressure on the points is an issue that is not yet resolved, but we estimate that the pressure is about the same in both the $\Delta T-I$ experiment and the differential conductance experiments.

Issues of surface planarity, interpretation of the effective number of contact points, and the difficulty of ascertaining contact pressure and contact tip radius, make quantitative predictions of microscopic single point parameters very difficult. Further investigations in quantifying these parameters are in progress. We are also studying the effects in sharp tips with tip radius that are much smaller than the electron-phonon thermalization lengths.

The authors would like to thank M. Ketchen and J. Speidell at the IBM T. J. Watson Research Center for their technical advice and guidance that enabled an expeditious completion of this experiment. The authors would also like to thank J. Sharp at Marlow Industries, Inc. for providing the tiny thermoelectric cooler.

¹G. Nolas, J. Sharp, and H. Goldsmid, *Thermoelectrics: Basic Principles and New Materials Development* (Springer, Berlin, 2001).

²F. J. DiSalvo, *Science* **285**, 703 (1999).

³R. Venkatasubramanian, E. Silvola, T. Colpitts, and B. O'Quinn, *Nature* (London) **413**, 597 (2001).

⁴Y. S. Ju and U. Ghoshal, *J. Appl. Phys.* **88**, 4135 (2000).

⁵V. Zakordonets and G. Loginov, *Semiconductors* **31**, 265 (1997).

⁶M. Bartkowiak and G. Mahan, *Mater. Res. Soc. Symp. Proc.* **545**, 265 (1999).

⁷D. Polvani, J. Meng, N. Chandra Shekar, J. Sharp, and J. Badding, *Chem. Mater.* **13**, 2068 (2001).

⁸A precision bare K -type $50 \mu\text{m}$ wire diameter thermocouple from Omega Engineering, Inc. was used in the experiment.